http://dx.doi.org/10.5012/bkcs.2013.34.1.89

Adipic Acid Assisted Sol-Gel Synthesis of $Li_{1+x}(Mn_{0.4}Ni_{0.4}Fe_{0.2})_{1-x}O_2$ ($0 < x < 0.3$) as Cathode Materials for Lithium Ion Batteries

Kaliyappan Karthikeyan, Samuthirapandian Amaresh, Ju-Nam Son, Shin-Ho Kim, Min-Chul Kim, Kwang-Jin Kim, Sol-Nip Lee, and Yun-Sung Lee*

Faculty of Applied Chemical Engineering, Chonnam National University, Gwang-ju 500-757, Korea
**E-mail: leeys@chonnam.ac.kr*
Received August 27, 2012, Accepted October 5, 2012

Layered $Li_{1+x}(Mn_{0.4}Ni_{0.4}Fe_{0.2})_{1-x}O_2$ ($0 < x < 0.3$) solid solutions were synthesized using solgel method with adipic acid as chelating agent. Structural and electrochemical properties of the prepared powders were examined by means of X-ray diffraction, Scanning electron microscopy and galvanostatic charge/discharge cycling. All powders had a phase-pure layered structure with $R\bar{3}m$ space group. The morphological studies confirmed that the size of the particles increased at higher x content. The charge-discharge profiles of the solid solution against lithium using 1 M $LiPF_6$ in EC/DMC as electrolyte revealed that the discharge capacity increases with increasing lithium content at the 3a sites. Among the cells, $Li_{1.2}(Mn0_{.32}Ni_{0.32}Fe_{0.16})O_2$ (x = 0.2)/ Li^+ exhibits a good electrochemical property with maximum initial capacity of 160 $mAhg^{-1}$ between 2-4.5 V at 0.1 $mAcm^{-2}$ current density and the capacity retention after 25 cycles was 92%. Whereas, the cell fabricated with x = 0.3 sample showed continuous capacity fading due to the formation of spinel like structure during the subsequent cycling. The preparation of solid solutions based on $LiNiO_2$-$LiFeO_2$-Li_2MnO_3 has improved the properties of its end members.

Key Words : Sol-gel method, Layered oxides, Cathode materials, Li_2MnO_3, Iron doping

Introduction

Layered $LiCoO_2$ has been widely adopted as the positive electrode materials in lithium ion batteries (LIB) for commercial applications such as mobile phone, laptops and other customer electronic devices. Increasing the cell voltage and capacity of LIB is substantial to extend their potential application to large scales like hybrid electrical vehicles (HEV) and plug-in hybrid electric vehicles (PHEV). While $LiCoO_2$ showed excellent electrochemical behavior, the high cost and toxicity of cobalt leads to lookout for the alternatives such as $LiMO_2$ (M = Ni or Mn) and Li_2MnO_4.[1] Although there has been much works focused on the optimization of Ni and Mn based cathode materials, the troubles still remain for adopting them in practical applications.[2-4] The olivine type $LiFePO_4$ is a promising cathode material for LIB due to its low cost and stable cyclic performance. But, low electronic conductivity and low cell voltage (~3 V) of $LiFePO_4$ confined its possibility to utilize in HEVs.[5] The selection of positive electrode materials with high lithium content is an effective way to increase the cell capacity and voltage, which can be used in larger scale applications. Layered manganese oxide (Li_2MnO_3) has attracted much attention as alternative cathode for LIB due to its high lithium content, less cost, low toxic nature than $LiCoO_2$. Unfortunately, the oxidation state of Mn in Li_2MnO_3 is fixed as 4+ and it cannot be further oxidized beyond to Mn^{5+} state in an octahedral oxygen environment.[6] Moreover, the extraction of two lithium ions from its structure during charging and reinsertion of only one lithium ion during discharging limits the overall capacity of the cell to store charge. To surpass this problem, a new concept of preparing one and one solid solution between Li_2MnO_3 and $LiMO_2$ (M = Ni, Co or Cr) such as $Li[Li_{(1-2x)/3}Ni_xMn_{(2x)/3}]O_2$ and $Li[Li_{(1-x)/3}Co(Cr)_xMn_{(2-2x)/3}]O_2$ has been studied.[7-11] The structure of the above mentioned solid solutions was stabilized by Co^{3+} or Cr^{3+} that partially replaced Li^+ and Mn^{4+} in $Li[Li_{1/3}Mn_{2/3}]O_2$, while maintaining the oxidation state of other remaining Mn atoms in the 4+ state. Inspite of delivering improved structural and electrochemical behavior, the toxic nature of Cr and Co hindered those materials to be utilized in larger scale LIB applications.

Compared with lithium metal oxides containing cobalt, nickel, and chromium in layered solid solutions, lithium-iron oxides have advantages in terms of reduced costs and toxicity. Recently, Tabuchi *et al.* have proposed a series of iron containing Li_2MnO_3 ($Li_{1+x}(Fe_yMn_{1-y})_{1-x}O_2$, $0 \le x \le 1/3$, $0.3 \le y \le 0.7$) layered material as new class of cathode materials for LIB.[12,13] Because of its lower discharge voltage and capacity (> 80 $mAhg^{-1}$), these materials may not be used for LIB in large scale application. Of late, the same group reported the nickel and iron substituted Li_2MnO_3 ($Li_{1+x}[(Fe_{1/2}Ni_{1/2})_yMn_{1-y}]_{1-x}O_2$, $0 < x < 1/3$, $0.2 \le y \le 0.8$) with and improved electrochemical performance.[14] Although these materials were prepared with good structural properties, it exhibited poor cycling performance due to its synthesis conditions. Since these materials were prepared using a combination of co-precipitation-hydrothermal-solid state methods, the electrochemical performance for long term cycling was affected. Moreover, hydrothermal step is a com-

plicated process and an oxidizer was also used additionally, which can increase the production cost. Due to the depletion of natural oil resources and increase in market demand for HEVs and PHEVs, it is necessary to develop low cost and environmental friendly energy source material by simple preparation methods. In our previous work, we prepared a series of low cost and green $Li_{1+x}(Mn_{0.4}Ni_{0.4}Fe_{0.2})_{1-x}O_2$ ($0 < x < 0.3$) cathode material using simple adipic acid (AA) assisted sol-gel method for advanced LIB application. Among the materials prepared, $Li(Li_{0.2}Mn_{0.32}Ni_{0.32}Fe_{0.16})O_2$ ($x = 0.2$) with 1 M AA at 700 °C exhibited better electrochemical performance with improved cycling behavior.[15] In this work, we report the optimization of x value in ($Li_{1+x}(Mn_{0.4}Ni_{0.4}Fe_{0.2})_{1-x}O_2$ ($0 < x < 0.3$)) and their effect on its battery performance. These composite materials have the advantages of three end members such as high capacity of $LiNiO_2$, low cost of $LiFeO_2$ and good thermal stability of Li_2MnO_3.

Experimental

A sol-gel method was adopted to synthesis $Li_{1+x}(Mn_{0.4}Ni_{0.4}Fe_{0.2})_{1-x}O_2$ ($0 < x < 0.3$) powders using adipic acid as chelating agent. A desired amount of $Li(CH_3COO)\cdot 2H_2O$ (Wako, Japan), $Ni(CH_3COO)_2\cdot H_2O$ (Aldrich), $Fe(CH_3COO)_2\cdot H_2O$ (Aldrich), and $Mn(CH_3COO)_2\cdot 4H_2O$ (Aldrich) were dissolved in triple distilled water, and added drop wise to a continuously stirred aqueous solution of AA (Aldrich). The molar ratio of AA to total metal ions was unity. The pH of the reaction mixer was adjusted to seven using ammonium hydroxide (NH_4OH) solution. The resultant solution was heated at 80 °C until a transparent sol was obtained. As the water evaporated further, the sol transforms into a viscous transparent gel. The resulting precursors were decomposed at 400 °C for 2 h in order to eliminate the organic components. The final product was obtained by the calcination of decomposed powders at 700 °C for 10 h in air.

The phase purity of the prepared powders was examined by X-ray diffraction measurement (Rint 1000 Rigaku, Japan) using Cu Kα radiation. The surface morphological features of the powders were observed by FE-SEM analysis (S-4700 microscope, Hitachi, Japan) and transmission electron microscopy (TEM, TecnaiF20, Philips, Holland). Cyclic voltammetry (CV) and electrochemical impedance spectroscopy (EIS) measurements were carried out using an electrochemical analyzer (SP-150, Bio-Logic, France). The charge/discharge test (C-DC) was performed in CR2032 type cell. The cathodes for the coin cell were prepared by pressing the mixture of 20 mg of prepared materials, 3 mg of Ketjen black and 3 mg of Teflonized acetylene black (TAB) mixture on 150 mm^2 nickel mesh and dried at 160 °C for 4 h in a vacuum oven. The test cells were fabricated in an argon filled glove box by pressing a cathode and lithium metal anode separated by a porous polypropylene separator (Celgard 3401). 1 M $LiPF_6$ in 1:1 EC/DMC (v/v) was used as electrolyte. The cell was charged/discharged at 10 $mAcm^{-2}$ current density between 2-4.5 V at ambient temperature.

Results and Discussion

The XRD patterns of $Li_{1+x}(Mn_{0.4}Ni_{0.4}Fe_{0.2})_{1-x}O_2$ ($0 < x < 0.3$) powders prepared using AA assisted sol-gel method were presented in Figure 1(a). The diffraction patterns of all samples were similar with no impurity peaks, which are attributed from the homogeneous atomic scale mixing of the starting materials. The additional less intense peaks between $2\theta = 21$-$25°$ were considered to be attributed to the formation of monoclinic $Li[Li_{1/3}Mn_{2/3}]O_2$ phase ($C2/m$). The superlattice ordering resulted from the short-range ordering of Li, Fe, Ni, and Mn atoms in the transition metal layers.[7,10,15,16] The layered characteristic behavior of the materials was

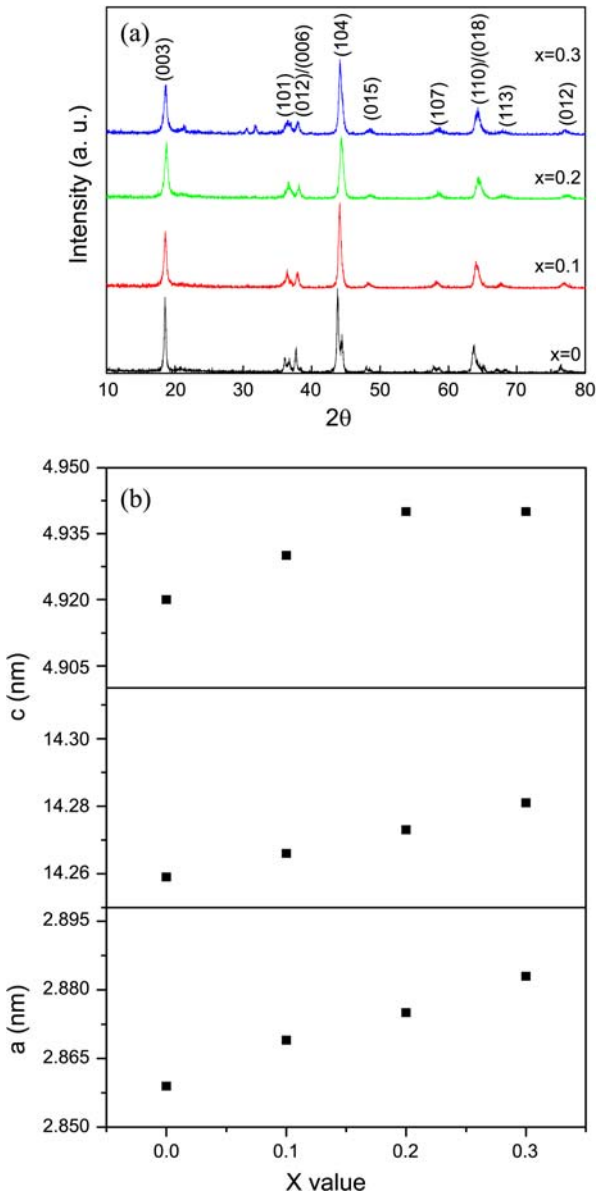

Figure 1. (a) XRD patterns of $Li_{1+x}(Mn_{0.4}Ni_{0.4}Fe_{0.2})_{1-x}O_2$ ($0 < x < 0.3$) powers synthesized using adipic acid assisted sol-gel method at 700 °C (b) Variation of lattice parameter with x content.

increased with increasing x value, which was confirmed by the disappearance of the shoulders for (1 0 1) and (1 0 4) peaks as well as the clear splitting of hexagonal doublets.[13-15] Therefore, all the patterns were able to be indexed based on a hexagonal α-$NaFeO_2$ (with space group of *R3m*) layered structure along with some additional peaks caused by monoclinic distortion.[12,15] The lattice parameters for all samples were calculated based on hexagonal structure and presented as plot against x value in Figure 1(b). The values of a and c are slightly larger with increasing x value, demonstrating the effect of lithium substitution on the structural parameters. According to the effect of ionic radii proposed by Shannon.[17] the radius of Li^+ (0.76 Å) is larger than that of Ni^{2+} (0.69 Å), Fe^{3+} (0.69 Å) and Mn^{4+} (0.53 Å, six-fold coordination). Since the radius of Li^+ is larger, the substitution of Li^+ for metal ions causes the increase in lattice parameters. Moreover, the c/a ratio of all samples is more than 4.9, indicating the good layered behavior of synthesized samples. It is well known that with increasing *c/a* ratio beyond 4.90, the ordering of the layered structure increases and the crystal structure becomes more hexagonal.[4] However, it is well known that the c/a value and cation mixing amount showed change with increase in Ni content. The higher Ni content resulted in worse hexagonal ordering along with a higher cation mixing. Among the sample, the sample with x = 0.2 has the $I_{(0\,0\,3)}/I_{(1\,0\,4)}$ ratio of about 0.84, which is also agreement with the value reported by Ohzuku *et al.* (0.84).[3] This is clearly indicated that there may be a small proposition of Ni and Li ions undergo interchange of sites in the crystal lattice. It is believed that the fractional cation mixing may not lead to the formation of inactive rock-salt domains that affects the electrochemical property.[15]

Figure 2 illustrated the surface morphology of powders prepared with different x values at 700 °C. From Figure 2, it is clearly revealed that the particle size gets increased with increase in x value, which may be due to the incorporation of high lithium into the crystal lattice that leads to the crystal growth. As can be seen from Figure 2(a) and 2(b) that the sample with low x content (0 and 0.1) showed uneven morphology and size distribution, while the sample with x = 0.3 exhibited flake like morphology and the flakes are stacked over each other forming a bigger molecule. Among the powders prepared, the sample with x = 0.2 has the particles of around 95 nm size with uniform size distribution. It was proposed that the small particles of 100 nm size with even distribution is beneficial for better Li^+ diffusion and enhanced electronic transport at high current rates.[18,21] The small particles of 10-20 nm size observed on the surface of all sample in Figure 2 could be considered as carbon.

The TEM analysis performed confirms the presence of carbon on the surface of the particles and the images of x = 0.2 sample was given in Figure 3. Figure 3(a) clearly demonstrated that the uniform size distribution of the particles with the size of around 80-100 nm are observed, which is correlated well with the SEM studies. It can be seen more clearly from Figure 3(b) that a nanolayer amorphous carbon is coated on the surface of particles, which was attributed to the carbonization of adipic acid during the heat treatment process. In addition, the degree of homogeneity of the sample with x = 0.2 was also confirmed using TEM analysis. Figure

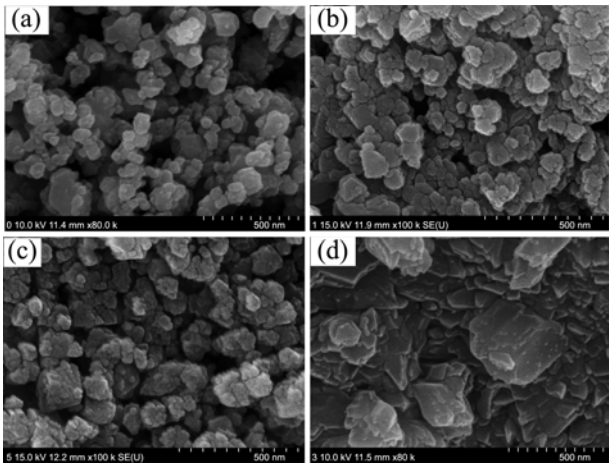

Figure 2. SEM images of $Li_{1+x}(Mn_{0.4}Ni_{0.4}Fe_{0.2})_{1-x}O_2$ ($0 < x < 0.3$) powers with different x value (a) x = 0 (b) x = 0.1 (c) x = 0.2 and (d) x = 0.3.

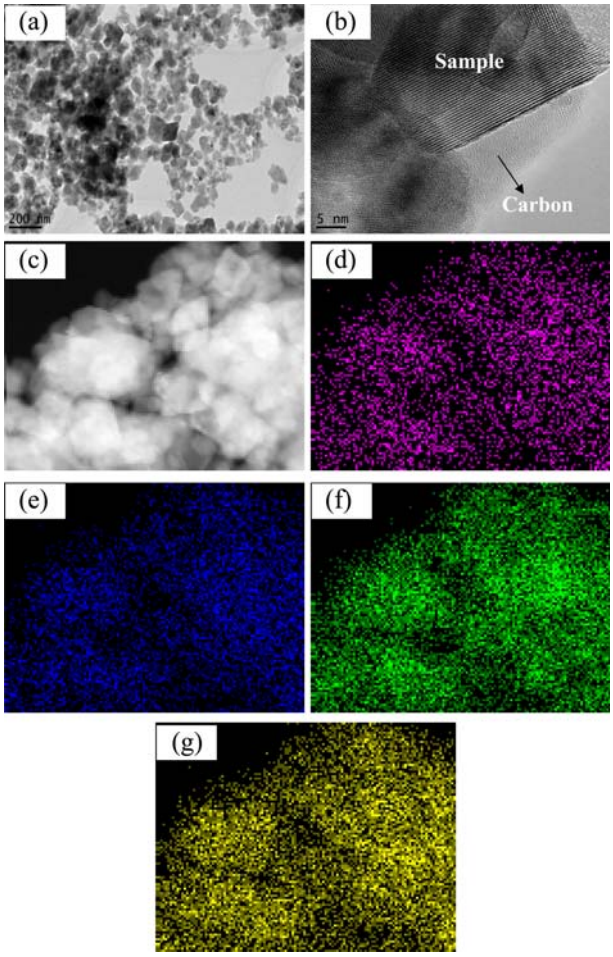

Figure 3. TEM images of (a and c) $Li_{1.2}(Mn_{0.32}Ni_{0.32}Fe_{0.16})O_2$ particles with 1 M adipic acid, (b) presence of carbon on the surface of the particles. (d) Mapping of C, (e) mapping of Fe, (f) mapping of Mn and (g) mapping of Ni.

3(d)-3(g) illustrated the metal ions distribution with similar intensities corresponding to the mapping area as shown Figure 3(c), indicating the molecular level mixing of the starting materials. Furthermore, it can be concluded from the Figure 3(d) that the uniform distribution of the carbon on the surface of the samples.

The C-DC studies of the cells fabricated were performed between 2-4.5 V at 0.1 $mAcm^{-2}$ current density and the corresponding initial C-DC curves of $Li/Li_{1+x}(Mn_{0.4}Ni_{0.4}Fe_{0.2})_{1-x}O_2$ ($0 < x < 0.3$) cells were presented in Figure 4(a). The electrochemical charging process of all cells occurred in two dominant stages as evident in Figure 4(a). During the first stage, a smooth charging profile started at open circuit voltage and uniformly increases to 3.7 V and then, the charging of the cells holds at 3.8 V where the oxidation of Ni^{2+} to Ni^{4+} occurred.[19] In the second stage, a voltage plateau above 4.45 V was observed, which was mainly due to the electrochemical removal of Li_2O from the structure associated with the active oxygen loss from the lattice.[7,8,20] The removal of Li_2O from the structure at high potential range yields an electrochemically active MnO_2 component, which is responsible for maximizing the discharge capacity. It can also be seen from the Figure 4(a) that the flat charging plateau over 4.45 V gets increased with increase in x value up to 0.2 and then slightly decreases, which is the main characteristic behavior of a solid solution in the higher Li_2MnO_3 content. It is worth mentioning here that the Fe ions did not oxidize or reduce during the C-DC process, which was confirmed by the disappearance of a voltage plateau around 4 V, resulting from the partial cation mixing between the transition metal layers by Fe ions.[5,13,15] Meanwhile, the manganese ions did not participate in the electrochemical process due to the limitation of oxidation stage of Mn^{4+} to form Mn^{5+}.[5,6] From the above observation, it was concluded that both Mn and Fe acted as inactive members to stabilize the Ni redox reaction in the crystal structure of $Li_{1+x}(Mn_{0.4}Ni_{0.4}Fe_{0.2})_{1-x}O_2$ ($0 < x < 0.3$) solid solutions during intercalation/de-intercalation.[5,13-15] Although a large irreversible capacity (ICL) loss was observed for all cells, a columbic efficiency of over 99% was achieved after second cycle irrespective of samples tested. During the first charge, the $Li_{1-z}Ni_{1+z}O_2$ structure (α-$NaFeO_2$ system) was destroyed due to the deintercalation of Li^+ from unstable 3a site and the total quantity of Li^+ for intercalation for first discharge will be limited, which leads to the large ICL.[21] The x content also affected the discharge profile as shown in Figure 4(a). A smooth downward discharge curve was obtained for the samples x = 0 and 0.1. An additional discharge plateau was observed for the samples with x content 0.2 and 0.3 which was not detected for the samples with high Fe content. Although the origin of the plateau is still unknown, it was also observed in previous studies.[13-15] Among the cells, the $Li_{1.2}(Mn_{0.32}Ni_{0.32}Fe_{0.16})_2/Li^+$ cell delivered the highest discharge capacity of 160 $mAhg^{-1}$, while the sample with x = 0 delivering the lowest capacity of 106 $mAhg^{-1}$ at 0.1 $mAcm^{-2}$ current density. The samples prepared with x = 0.1 and 0.3 delivered a capacity of 138 and 144 $mAhg^{-1}$, respectively,

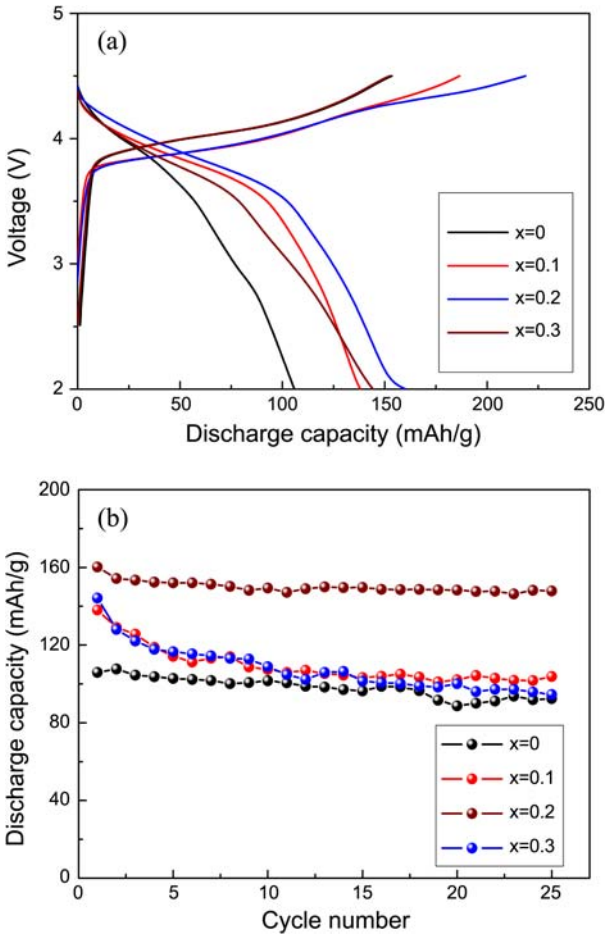

Figure 4. (a) Initial charge discharge curves of $Li_{1+x}(Mn_{0.4}Ni_{0.4}Fe_{0.2})_{1-x}O_2$ ($0 < x < 0.3$)/Li^+ cells at 0.1 $mAcm^{-2}$ current density between 2-4.5 V in 1 M $LiPF_6$/1:1 EC/DMC electrolyte and (b) the cyclic behavior of the cells with various x content for 25 cycles.

at the same current density. The highest capacity of $Li_{1.2}(Mn_{0.32}Ni_{0.32}Fe_{0.16})_2/Li^+$ cell was attributed from its well-defined structure with uniform particle size and distribution of the cathode material. Since the morphological feature of any material directly affects its electrochemical performance, the capacity of the samples linearly increased and then decreased at higher x content. It was reported that the materials with around 100 nm size could be exhibit a better lithium ion diffusivity,[15,18,22] and hence the sample prepared with x = 0.2 delivered an enhanced capacity, which correlated well with the SEM and TEM results. The cyclic behavior of $Li_{1+x}(Mn_{0.4}Ni_{0.4}Fe_{0.2})_{1-x}O_2$ ($0 < x < 0.3$)/Li^+ cells were presented in Figure 4(b). As seen from Figure 4(b), the cyclic behavior of the cell strongly depends on its structural integrity. Since the structural integrity of the sample prepared with x = 0.2 was high, it delivered maximum capacity of 160 $mAhg^{-1}$ in the first cycle and maintained about 148 $mAhg^{-1}$ capacity after 25 cycles at 0.1 $mAcm^{-2}$ current density, which corresponds to the retention of 92%. While the sample prepared with x = 0, 0.1 and 0.3 showed a capacity retention of about 87, 75 and 67%, respectively. The excellent cyclic behavior of $Li_{1.2}(Mn_{0.32}Ni_{0.32}Fe_{0.16})O_2/Li^+$ could be attributed to its

well defined structure and size. The poor cycling behavior of the sample prepared with x = 0.3 may be the result of its uneven particle shape, which hinder the lithium mobility and also from the formation of spinel-like oxides during the subsequent cycling process.[23,24] The formation of $LiFeO_2$ or $LiMnO_2$ made the particles to undergo structural changes during the C-DC process, resulting in the dissolution of Mn or Fe ions in electrolytes. This reduced the amount of activators such as Mn and Fe ions, which is used for stabilizing the structure of $Li_{1.3}(Mn_{0.28}Ni_{0.28}Fe_{0.12})O_2$ and hence the continuous capacity fading occurred.[14,25,26] It was also reported that the substitution of small amount of 3d metal cations has remarkably improved its electrochemical cycling performance by reducing faster lithium ion intercalation/deintercalation.[13,15] The cycling test of the cells with different x value clearly revealed that the stabilization of charge-discharge curves during the cycling process is attributed to the advantages of both Fe and Ni inclusions in Li_2MnO_3.[5,7,12,14] These results clearly demonstrated that x = 0.2 is an optimum value for $Li_{1+x}(Ni_{0.4}Mn_{0.4}Fe_{0.2})_{1-x}O_2$ active materials, which is well agreed with the previous reports for layered materials.[4,12,13,15]

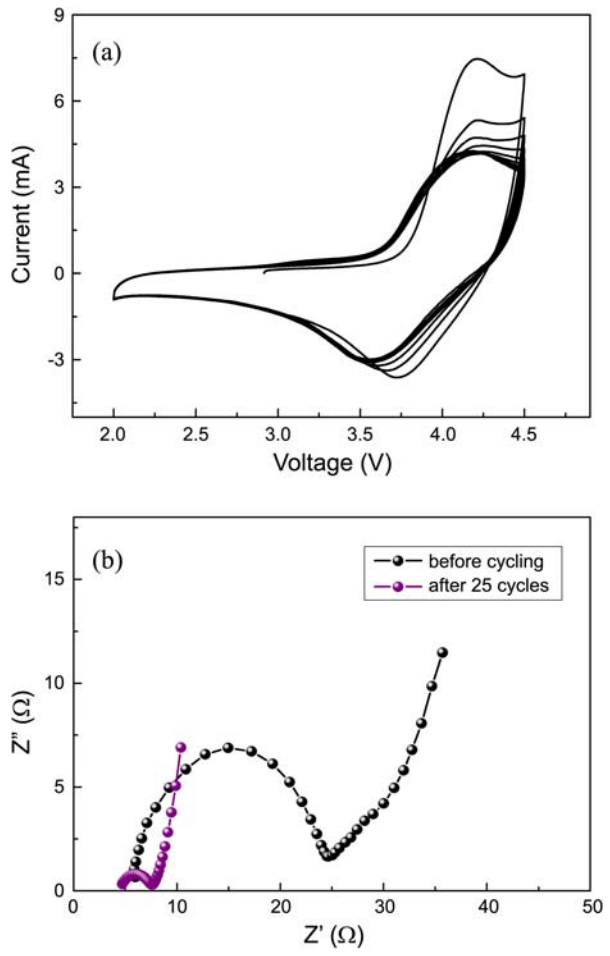

Figure 5. (a) CV curves of $Li_{1.2}(Mn_{0.32}Ni_{0.32}Fe_{0.16})O_2/Li^+$ cell recorded at 0.5 mV/s scan rate between 2-4.5 V for 15 cycles (b) Nyquist spectrum of $Li_{1.2}(Mn_{0.32}Ni_{0.32}Fe_{0.16})O_2/Li^+$ cell before and after cycled at 0.1 $mAcm^{-2}$ current density.

The cyclic voltammetry of $Li_{1.2}(Mn_{0.32}Ni_{0.32}Fe_{0.16})O_2/Li^+$ cell conducted between 2-4.5 V at 0.5 mVs^{-1} for 15 cycles and corresponding CV traces were presented in Figure 5(a). As seen from Figure 5(a), there is an appearance of one anodic peak around at 4.2 V during charging process and corresponding reduction peak is observed at 3.6 V on discharge corresponding to the oxidation of Ni^{2+} to Ni^{4+} and the subsequent reduction of Ni^{4+} in the solid solution.[27] It is noted from CV curve that there is no cathodic peak observed around ~3 V, indicating Mn^{3+}/Mn^{4+} redox couple does not involve in the electrochemical reaction during the C-DC process.[7] Moreover, no redox peaks corresponding to the $Fe^{3+/4+}$ was observed within the recorded potential range, clearly demonstrating that Mn and Fe are electrochemically inactive and are mostly used to stabilize the $Li_{1.2}(Mn_{0.32}$-$Ni_{0.32}$ $Fe_{0.16})O_2$ structure. It is also found that the intensity of the CV curves become low during the subsequent cycles. The decrease in peak intensity may arise from the cation mixed during the initial few cycles. From the fourth cycle onwards, the CV traces are almost overlapped, revealing an excellent electrochemical reversibility of lithium ions during the C-DC process in $Li_{1.2}(Mn_{0.32}Ni_{0.32}Fe_{0.16})O_2$ compound. The higher reversibility of $Li_{1.2}(Mn_{0.32}Ni_{0.32}Fe_{0.16})O_2$ electrode might be attributed to the small particles with uniform distribution and good contact between the particles, which facilitate the Li-ion diffusion enormously, thereby enhanced its electrochemical behavior.[15,18,21]

The Nyquist plots of $Li_{1.2}(Mn_{0.32}Ni_{0.32}Fe_{0.16})O_2/Li^+$ cell recorded before and after cycling at 0.1 mAg^{-1} between 2-4.5 V was illustrated in Figure 5(b). In Figure 5(b), the semicircle at high frequency region represents the impedance associated with the formation of solid state interface (solution resistance, R_s) layer between the surface of electrode and electrolyte and the semicircle is corresponding to a faradaic charge transfer resistance at the interface as well as its relative double layer capacitance. The inclined part at the low frequency end is a Warburg tail that implies the lithium ion diffusion control process between the electrode-electrolyte interfaces.[15] A small variation in R_s was observed upon cycling from the impedance spectrum, which could be neglected.[15,28] According to the Suresh *et al.* this small variation in R_s value was attributed to the formation of insulating film consisting of lithium compounds on surface of the electrode.[29] As well as, the variation was also resulted from the destruction and modification of SEI layer due to current flux during the C-DC process.[30] Since the chemistry of lithium ions present in electrolyte is complicated, this complex mechanism leads to poor contact between the conducting species in the electrolyte, which also results in a slight variation in R_s.[31,32] Furthermore, the large difference in the charge transfer resistance (R_{ct}) after cycling probably caused from the increase in electrode surface area due to the expansion and contraction process during the cycling.[33,34] It is mainly owing to the smaller size of particles, ensuring the reduction of diffusion path for lithium ions and thereby increasing the conductivity, which will contribute to reduce the R_{ct} and hence its cycling performance was improved.

These discussions were well agreed with the results obtained from the SEM and C-DC studies.

Conclusion

A series of green $Li_{1+x}(Mn_{0.4}Ni_{0.4}Fe_{0.2})_{1-x}O_2$ ($0 < x < 0.3$) composites were prepared using adipic acid assisted solgel method and their potential to utilize as cathode materials for lithium ion batteries have been studied. Among the materials synthesized, the composite with $x = 0.2$ exhibited excellent electrochemical performance with enhanced cyclic behavior. This improved performance was attributed to its well-ordered layered structure and small particles with uniform size distribution. These layered materials containing iron could be used as low cost and eco-friendly energy source materials for large scale lithium ion batteries application.

Acknowledgments. This study was financially supported by Chonnam National University, 2010.

References

1. Breger, J.; Dupré, N.; Chupas, P. J.; Lee, P. L.; Proffen, T.; Parise, J. B.; Grey, C. P. *J. Am. Chem. Soc*. **2005**, *127*, 7529.
2. Guyomard, D.; Tarascon, J. M. *Solid-State Ionics* **1994**, *69*, 222.
3. Ohzuku, T.; Makimura, Y. *Chem. Lett.* **2001**, *8*, 744.
4. Ammundsen, B.; Paulsen, J.; Davidson, I.; Liu, R. S.; Shen, C. H.; Chen, J. M.; Jang, L. Y.; Lee, J. F. *J. Electrochem. Soc.* **2002**, *149*, A431.
5. Ammundsen, B.; Paulsen, J. *Adv. Mater.* **2001**, *13*, 943.
6. Padhi, A. K.; Najundaswamy, K. S.; Goodenough, J. B. *J. Electrochem. Soc.* **1997**, *144*, 1188.
7. Lu, Z.; Dahn, J. R. *J. Electrochem. Soc.* **2002**, *149*, A1454.
8. Park, Y. J.; Hong, Y. S.; Wu, X.; Kim, M. G.; Ryu, K. S.; Chang, S. H. *J. Electrochem. Soc.* **2004**, *151*, A720.
9. Arunkumar, T. A.; Wu, Y.; Manthiram, A. *Chem. Mater.* **2007**, *19*, 3067.
10. Thackeray, M. M.; Kang, S. H.; Johnson, C. S.; Vaughey, J. T.; Benedek, R.; Hackney, S. A. *J. Mater. Chem*. **2007**, *17*, 3112.
11. Sun, Y. K.; Kim, M. G.; Kang, S. H.; Amine, K. *J. Mater. Chem.* **2003**, *13*, 319.
12. Tabuchi, M.; Nabeshima, Y.; Takeuchi, T.; Tatsumi, K.; Imaizumi, J.; Nitta, Y. *J. Power Sources* **2010**, *195*, 834.
13. Tabuchi, M.; Nakashima, A.; Shigemura, H.; Ado, K.; Kobayashi, H.; Sakaebe, H.; Kageyama, H.; Kohzaki, M.; Hirano, A.; Kanno, R. *J. Electrochem. Soc.* **2002**, *149*, A509.
14. Tabuchi, M.; Nabeshima, Y.; Takeuchi, T.; Kageyama, H.; Tatsumi, K.; Akimoto, J.; Shibuya, H.; Imaizumi, J. *J. Power Sources* **2011**, *196*, 3611.
15. Karthikeyan, K.; Amaresh, S.; Lee, G. W.; Aravindan, V.; Kim, H.; Kang, K. S.; Kim, W. S.; Lee, Y. S. *Electrochim. Acta* **2012**, *68*, 246.
16. Kim, J. S.; Johnson, C. S.; Thackeray, M. M. *Electrochem. Commun.* **2002**, *4*, 205.
17. Shannon, R. D. *Acta Crystallogr. A* **1976**, *32*, 751.
18. Suryanarayana, C.; Koch, C. C. *Hyperfine Interact.* **2000**, *130*, 5.
19. Koyama, Y.; Tanaka, I.; Adachi, H.; Makimura, Y.; Ohzuku, T. *J. Power Sources* **2003**, *119*, 644.
20. Lu, Z.; MacNeil, D. D.; Dahn, J. R. *Electrochem. Solid State Lett.* **2001**, *4*, A191.
21. Wang, Z.; Sun, Y.; Chen, L.; Huang, X. *J. Electrochem. Soc.* **2004**, *151*, A914.
22. Suryanarayana, C. *Jom-J. Min. Met. Mat. S.* **2002**, *54*, 24.
23. Robertson, A. D.; Bruce, P. G. *Chem. Mater.* **2003**, *15*, 1984.
24. Kumagai, N.; Kim, J.; Tsuruta, S.; Kadoma, Y.; Ui, K. *Electrochim. Acta* **2008**, *53*, 5287.
25. Reed, J.; Ceder, G. *Electrochem. Solid State Lett.* **2002**, *5*, A145.
26. Kim, J.; Fulmer, P.; Manthiram, A. *Mater. Res. Bull.* **1999**, *34*, 571.
27. Wang, C. W.; Ma, X. L.; Cheng, J. L.; Zhou, L. Q.; Sun, J. T.; Zhou, Y. H. *Solid State Ionics* **2006**, *177*, 1027.
28. Liu, J.; Manthiram, A. *Chem. Mater.* **2009**, *21*, 16951.
29. Suresh, P.; Shukla, A. K.; Munichandraiah, N. *Materials Letters* **2005**, *59*, 953.
30. Shaju, K. M.; Rao, G. V. S.; Chowdari, B. V. R. *Electrochim. Acta* **2004**, *49*, 1565.
31. Aurbach, D.; Schechter, A. *Electrochim. Acta* **2001**, *46*, 2395.
32. Wu, X. M.; Li, X. H.; Wang, Z.; Xiao, Z. B.; Liu, J.; Yan, W. B. *Mater. Chem. Phys.* **2004**, *83*, 78.
33. Park, C. K.; Park, S. B.; Shin, H. C.; Cho, W. I.; Jang, H. *Bull. Korean Chem. Soc.* **2011**, *32*, 191.
34. Ho, C.; Raistrick, I. D.; Huggins, R. A. *J. Electrochem. Soc.* **1980**, *127*, 343.